Charge Allocation in Hybrid Electrical Energy Storage Systems

Qing Xie, *Student Member, IEEE,* Yanzhi Wang, *Student Member, IEEE,* Younghyun Kim, *Member, IEEE,*
Massoud Pedram, *Fellow, IEEE,* and Naehyuck Chang, *Fellow, IEEE*

Abstract—**A hybrid electrical energy storage (HEES) system consists of multiple banks of heterogeneous electrical energy storage (EES) elements placed between a power source and some load devices and providing charge storage and retrieval functions. For an HEES system to perform its desired functions of 1) reducing electricity costs by storing electricity obtained from the power grid at off-peak times when its price is lower, for use at peak times instead of electricity that must be bought then at higher prices, and 2) alleviating problems, such as excessive power fluctuation and undependable power supply, which are associated with the use of large amounts of renewable energy on the grid, appropriate charge management policies must be developed in order to efficiently store and retrieve electrical energy while attaining performance metrics that are close to the respective best values across the constituent EES banks in the HEES system. This paper is the first to formally describe the global charge allocation problem in HEES systems, namely, distributing a specified level of incoming power to a subset of destination EES banks so that maximum charge allocation efficiency is achieved. The problem is formulated as a mixed integer nonlinear program with the objective function set to the global charge allocation efficiency and the constraints capturing key requirements and features of the system such as the energy conservation law, power conversion losses in the chargers, the rate capacity, and self-discharge effects in the EES elements. A rigorous algorithm is provided to obtain near-optimal charge allocation efficiency under a daily charge allocation schedule. A photovoltaic array is used as an example of the power source for the charge allocation process and a heuristic is provided to predict the solar radiation level with a high accuracy. Simulation results using this photovoltaic cell array and a representative HEES system demonstrate up to 25% gain in the charge allocation efficiency by employing the proposed algorithm.**

Index Terms—**Charge allocation, charge management, energy efficiency, energy storage system (ESS), hybrid energy storage system (HESS).**

Q. Xie, Y. Wang, and M. Pedram are with the Department of Electrical Engineering, University of Southern California, Los Angeles, CA 90089 USA (e-mail: xqing@usc.edu; yanzhiwa@usc.edu; pedram@usc.edu).

Y. Kim and N. Chang are with the Department of Electrical Engineering and Computer Science, Seoul National University, Seoul 151-742, Korea (e-mail: yhkim@elpl.snu.ac.kr; naehyuck@elpl.snu.ac.kr).

M. Pedram and N. Chang are the co-corresponding authors.

I. INTRODUCTION

ELECTRICAL energy is a high-quality form of energy [2] in the sense that 1) it can be easily and efficiently converted to other forms of energy, and 2) it can be used to control other (lower quality) forms of energy. However, electricity generation and consumption are typically not matched with each other. From utility company's perspective, storing the excess energy avoids energy wastage and mitigates overinvestment in power generation facilities by shaving the power demand during peak usage hours. Electrical energy storage (EES) systems thus increase the availability of electrical energy, mitigate the supply-demand mismatches, and reduce the generation capacity required to meet the peak power demand [3]–[5]. From consumers' perspective, storing energy obtained from the grid or generated by local power generation sources (such photovoltaic modules) during off-peak hours and using the stored energy to reduce the usage of grid electricity during peak hours can result in sizeable cost savings [6], [7].

Conventional EES systems are mainly homogeneous, i.e., they consist of a single type of EES element. Unfortunately, none of the existing EES elements can satisfy all the desired performance metrics such as high power and energy density, low cost and weight per unit capacity, high round-trip efficiency, and long cycle life. This limitation prevents the adoption of a wide range of socially and economically useful technologies, such as the widely adopted grid-scale EES and electric vehicles (EVs). Hence, eliminating this limitation of homogeneous EES systems is the primary motivation of our paper. Hybrid electrical energy storage (HEES) systems address this fundamental shortcoming of the conventional homogeneous EES systems using a collection of heterogeneous EES elements that are suitably organized and accessed [8], [9]. Each type of the EES elements has its unique strength and weakness. The HEES system can exploit the strength of each type of the EES element and achieve a combination of performance metrics that is superior to that of any of its individual EES components. Appropriate charge management policies, including charge allocation, charge replacement, charge migration, and bank reconfiguration, are designed according to the source/load profiles and characteristics of the HEES systems, in order to achieve the near-optimal overall performance metrics [1], [10]–[16].

We start by introducing a generalized HEES architecture comprised of two representative types of EES elements (batteries and supercapacitors) connected by a charge transfer
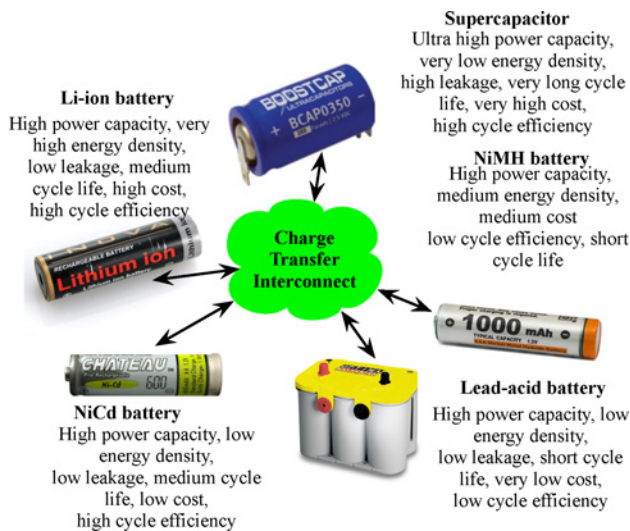
Fig. 1. Concept diagram of the HEES systems.

interconnect (CTI) and then build the corresponding electrical circuit models for power converters, and battery and supercapacitor banks. Next, we introduce the global charge allocation (GCA) problem for an HEES system, i.e., how to distribute the given source power supply to some selected EES destination banks in the HEES system so that the GCA efficiency[1] is maximized. This efficiency is determined by the characteristics of the selected banks and the magnitudes of the charging currents, and the states of charge (SoCs) of the banks. We consider the energy conservation and charge conservation during the charge allocation process. In addition to the energy pushed into all EES banks, we also take into account the power dissipation on the internal resistances of battery banks and supercapacitor banks, the power loss on chargers during the power conversion process, the rate capacity effect in batteries, and the self-discharge in supercapacitors.

The GCA problem may be decomposed into three subproblems.

1) What is the optimal voltage level setting for the CTI?
2) Which EES bank(s) should be selected among all the destination EES banks?
3) How should the charging current for each of the selected destination EES banks be assigned?

The GCA efficiency depends on the profile of the power source, magnitude of charging currents, and SoCs of each EES banks. Since SoCs of EES banks and the amount of source (input) power vary over time, and solutions to these three questions are interdependent, our method is an online, iterative approach. The charge allocation efficiency also depends on detailed characteristics of the external power source. We adopt a photovoltaic (PV) cell array as the incoming power source. An accurate forecast of the PV power is extremely important for us to develop for the GCA policy. We predict the solar radiation level based on the history of solar irradiance levels and the current observation.

---

[1]GCA efficiency is defined as the ratio between energy that is pushed into all EES banks and the total energy provided by all the power sources, during the whole charge allocation process for the EES system.

We formulate the GCA problem as a mixed-integer non-linear programming (MINLP) problem, which unfortunately cannot be optimally solved in polynomial time. We, therefore, break the whole charge allocation process into a series of time slots and at every decision epoch (which denotes the boundary between consecutive time slots), we solve an instantaneous charge allocation (ICA) problem, which seeks to optimize the charge allocation efficiency at a specific instance of time. The ICA problem is still an MINLP problem. However, we can simplify the ICA problem, and subsequently develop an effective way of solving the ICA problem in an iterative manner, where in each iteration the optimization problem is convex. We incorporate appropriate charging power limits for the high-charging-efficiency EES banks to the problem formulation to ensure that the charge allocation manager considers the future energy generation profile, and thus avoid greedy decisions that can result in significant future efficiency degradation. The charging power limits are derived using the Lagrange multiplier method to minimize the energy loss due to the rate capacity effect and self-discharge. The near-optimal solution of the original GCA problem is obtained by solving the ICA problem with charging power upper limit for high-charging-efficiency banks at every decision epoch throughout the charge allocation process. We record the ICA solutions to obtain the GCA solutions. Simulation results show that the percentage improvement of energy harvesting ability from various baseline setups ranges from 5% to 25% in general.

II. HEES SYSTEMS

A. Related Work

Considerable efforts have been invested in exploring the optimal architecture of the HEES systems. A direct-parallel connection of the battery and supercapacitor [17], [18] is simple but has major weaknesses because the shared terminal voltage of both sources must be kept same, which limits the capacity utilization of the supercapacitor and disables the active current distribution control. A cascade dc–dc converter between the battery and supercapacitor [19] can isolate the power sources and allow higher supercapacitor utilization. However, this design is targeted to a predefined charge management scenario whereby the supercapacitor is used as a battery buffer all the time. A more general architecture is a dc bus with distributed converters [20], [21]. However, the previous dc-bus architectures do not change the dc-bus voltage, which prevents them from achieving a higher system efficiency. The proposed HEES system resembles the dc-bus topology, but employs optimal control of the dc-bus voltage and does proper current distribution to each bank at run time.

Proper charge management on top of the hybrid EES architecture will be crucial if the architecture has some degree of freedom both at design and run times. A circuit model helps derive a desirable capacity ratio between the battery and supercapacitor, based on the peak power [22]. The configuration of a supercapacitor and the duty ratio as well as the pulse frequency of the load profile were considered in optimizing HEES performance in [23]. However, none of the previous work has introduced a general HEES management because the
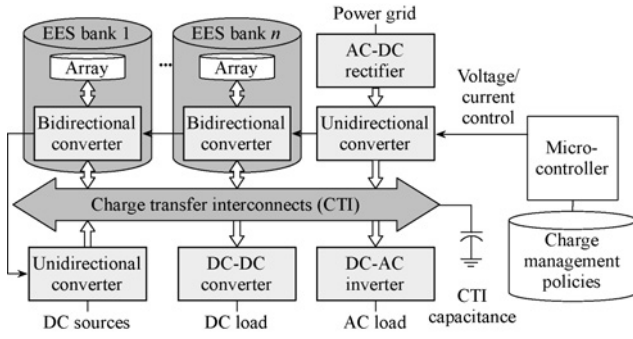
Fig. 2. Architecture of the proposed HEES system.

Fig. 3. Schematic of the charge allocation process in an HEES system.

previous HEES architectures are mostly dedicated to particular operation scenarios. In contrast, this paper presents the general form of the GCA problem, formulates it as a mathematical programming problem, and provides a near-optimal solution.

B. Motivation of HEES Systems

A conceptual drawing of the proposed HEES systems is depicted in Fig. 1. The system comprises of a number of heterogeneous EES banks, connecting to CTI through distributed power converters (not displayed in the figure). As we mentioned earlier, no existing EES elements fulfill all the requirements of an ideal energy storage system such as low capital cost, high cycle efficiency, long cycle life, low self-discharge rate, and high power and energy densities. Therefore, instead of relying on a single type of EES element technology, HEES systems use multiple heterogeneous EES elements.

Different types of EES elements have distinct characteristics. For example, a Li-ion battery bank has high energy capacity, low self-discharge, stable open terminal voltage, and relative low cost, but suffers from a low rate capability. In contrast, a supercapacitor bank has superior cycle efficiency, long cycle life, and high capability capability, but small energy density and high self-discharge rate. Therefore, heterogeneous EES banks, with properly designed charge management policies, can be used in a complementary manner to exploit the best characteristics (strengths) of each type of EES element, while hiding their weaknesses. The charge management policies include charge allocation [1], charge migration [10], [13], [16], charge replacement [12], and EES bank reconfiguration [11].

C. HEES System Architecture

Fig. 2 depicts the block diagram of the proposed HEES architecture. All heterogeneous EES banks are connected to each other via the CTI. An EES bank includes a set of homogeneous EES elements and a bidirectional converter since a typical EES element has a low voltage rating and a small energy capacity. These EES elements are organized in an appropriately constructed 2-D array using reconfigurable series and/or parallel connections. The bidirectional converters control the voltage and current when charging or discharging the EES array since there is generally a voltage difference between the CTI and the EES array. The bidirectional converters support the following two operation modes: 1) voltage regulation mode, the bidirectional converter generates a desirable output
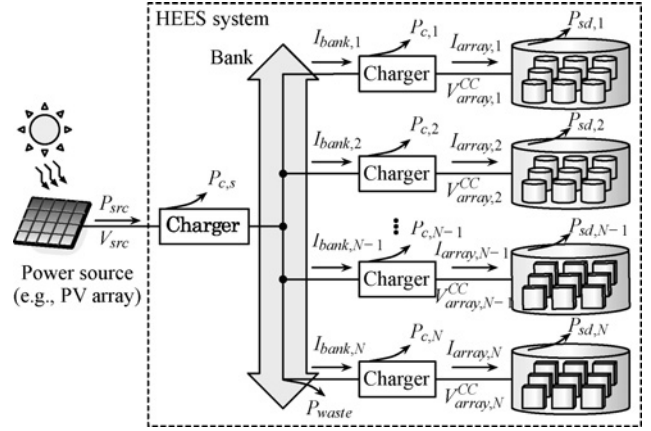
voltage regardless of the variation of the input power; and 2) current regulation mode, the bidirectional converter generates a desirable output current regardless of the variation of the input power. We refer to it as a charger if the converter is in this mode. The dc and ac power sources are connected to the HEES system using the unidirectional converters that only allow current flows onto the CTI. We use dc–dc converters and dc–ac inverters for the load devices to maintain the compatibility of the voltage levels between the CTI and load devices.

The charge management policies control the EES bank reconfiguration, CTI connection, CTI voltage, and charging currents/discharging current of each EES bank at each time instance in order to achieve the best HEES system performance. We control both the CTI voltage and charging/discharging current of EES arrays using the following method. We operate one converter in the voltage regulation mode to determine the desirable CTI voltage and all other converters in the current regulation mode. The output current for the voltage regulation converter is automatically determined since the total current flowing into CTI equals the total current flowing outward. This control scheme ensures the stability of CTI voltage and bank currents while we generate the software-level real-time tasks to implement the high-level charge management policies.

D. Charge Allocation Problem Statement

Charge allocation policy is used to determine the most suitable CTI voltage, a subset of EES banks, and the amount of charging current for each selected EES bank, in order to store the maximum amount of energy provided to the HEES system from a given power source, i.e., PV cells, a windmill, the power grid, and so on. The optimal charge allocation policy depends on the energy generation profile, i.e., it ideally distributes the incoming power at each time instance to the selected destination banks and achieves the highest possible GCA efficiency, which means that the maximum amount of energy is pushed into the selected EES banks. Thus, the prediction of the energy generation profile is important when attempting to determine the optimal charge allocation policy. Note that the charge allocation policy is also affected by the accuracy of the load profile prediction. This problem, however, falls outside the scope of this paper.

TABLE I
NOTATION USED IN SECTIONS II AND III-B

Notation	
S	full set of all EES banks in an HEES system
$S'(t)$	selection set among all EES banks in an HEES system
$\mathrm{SoC}_k(t)$	state of charge of the kth EES array
$V_{\mathrm{array},k}^{\mathrm{OC}}(t)$	open-circuit voltage (OCV) of the kth EES array
$V_{\mathrm{array},k}^{\mathrm{CC}}(t)$	closed-circuit voltage (CCV) of the kth EES array
$V_{\mathrm{cti}}(t)$	voltage level on the charge transfer interconnect
$V_{\mathrm{src}}(t)$	output voltage at the terminal of the power source
$P_{c,s}(t)$	power loss in sth source-to-CTI charger
$P_{c,k}(t)$	power loss in charging control charger in the kth EES bank
$P_{\mathrm{sd},k}(t)$	power loss due to the self-discharge in the kth EES bank
$I_{\mathrm{bank},k}(t)$	bank charging current of the kth bank, seen at the input of charger
$I_{\mathrm{array},k}(t)$	array charging current of the kth bank, seen at the output of charger
$P_{\mathrm{waste}}(t)$	excessive amount of input power that cannot be allocated to any EES banks

Fig. 3 shows a conceptual diagram of the charge allocation subsystem in an HEES system. Table I lists the important notations used in the following text. The system contains N heterogeneous EES banks, each of which consists of a number of homogeneous EES elements. Each EES bank is connected to the CTI through a charger. Supposing a charge allocation process starts at time $t = 0$ and ends at time $t = T_a$, for all $t \in [0, T_a]$, a subset $S'(t) \subseteq S$ is selected among the N EES banks to receive energy from the power sources through the CTI and the intervening chargers.

The source-to-CTI charger supports high voltage and current levels and regulates the output voltage of the power source $V_{\mathrm{src}}(t)$ to CTI voltage $V_{\mathrm{cti}}(t)$ through a feedback loop, subjecting to a conversion power loss of $P_{c,s}(t)$. The current flows from the source, through the CTI, into (a selected set) of chargers that connect the CTI and the destination EES banks. Since $V_{\mathrm{cti}}(t)$ affects the conversion efficiency of the power converters, choosing the optimal $V_{\mathrm{cti}}(t)$ is crucial for the charge allocation problem. The kth charger converts the *bank charging current* $I_{\mathrm{bank},k}(t)$ to *array charging current*, $I_{\mathrm{array},k}(t)$, with a power loss of $P_{c,k}(t)$. Note that the *open-circuit voltage* (OCV) of the kth EES array $V_{\mathrm{array},k}^{\mathrm{OC}}(t)$ is normally used when discussing the battery status; however, the *closed-circuit voltage* CCV of the kth EES array $V_{\mathrm{array},k}^{\mathrm{CC}}(t)$ is the voltage that we should consider for the accompanying circuits. The relationship between $V_{\mathrm{array},k}^{\mathrm{OC}}(t)$ and $V_{\mathrm{array},k}^{\mathrm{CC}}(t)$ will be discussed in Section III-A. The self-discharge rate of the kth EES bank $P_{\mathrm{sd},k}(t)$ also depends on the SoC and bank properties. In case that the input power exceeds the maximum receiving capability of the HEES system, the excess input power $P_{\mathrm{waste}}(t)$ cannot be stored and must be dumped to the ground (dissipated as heat). A formal definition of the charge allocation efficiency is presented in Section III-B.

III. PROBLEM FORMULATION

A. System Models

Table II lists the important notations used in the following text.

1) PV Model: The output power of the PV module P_{pv} is mainly determined by the voltage and the current of the PV module, V_{pv} and I_{pv}, the solar radiation level G, the

TABLE II
NOTATION USED IN SECTIONS III-B AND IV

| Notation	
P_{pv}	output power of the PV module, obtained using MPTT technique [24]
$C_{b,\mathrm{full}}$	total charge of battery when it is fully charged
C_b	remaining charge of a battery
γ_c	Peukert constant of the battery for charging process
C_{cap}	capacitance of supercapacitor banks
τ	self-discharge time constant of the supercapacitor bank
x_c	binary indicator of the charger status (on/off)
$P_{\mathrm{src}}(t)$	output power at the terminal of the power source
$P_{\mathrm{cti}}(t)$	power that is allocated from CTI to all EES banks
$P_{\mathrm{gain},k}(t)$	rate of energy increase in the kth EES array
$I_{\mathrm{eq},k}(t)$	equivalent charging current of the kth EES array, accounting for the rate capability and is the rate at which the remaining capacity of battery changes
$I_{\mathrm{sd},k}(t)$	self-discharge current in the kth EES array
η_{GCA}	global charge allocation efficiency
η_{ICA}	instantaneous charge allocation efficiency
$E_{\mathrm{HEES}}(t)$	energy stored in the HEES system, including all banks
$E_k(t)$	energy stored in the kth EES bank
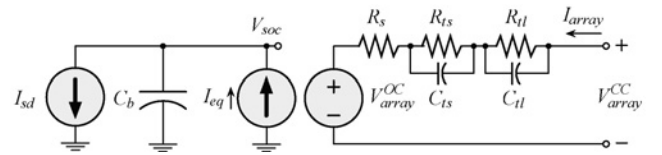
Fig. 4. Li-ion battery equivalent circuit model [30].

dark saturation current $I_0(T)$, the panel series and parallel resistances, R_s and R_p, the diode ideality factor A (which is a measure of how closely the diode follows the ideal diode equation), and the number of series-connected cells in that PV module N_s. The output power level can be written as

$$P_{\mathrm{pv}} = V_{\mathrm{pv}} \left(I_L(G) - I_0(T)(e^{\frac{(V_{\mathrm{pv}} + I_{\mathrm{pv}} R_s)q}{A N_s K T}} - 1) - \frac{V_{\mathrm{pv}} + I_{\mathrm{pv}} R_s}{R} \right). \quad (1)$$

In this paper, the PV module is used as the power source and connected to the HEES system through the CTI. We apply the maximum power transfer tracking (MPTT) [24] technique to maximize the input power transferring from the PV module to the CTI. We predict the solar radiation level G in (1) based on the observation of solar radiation level in Los Angeles, CA [25], while the other parameters are taken from [26].

2) Battery Bank: Battery banks have the advantages of high energy capacity and low self-discharge, and therefore, they are suitable for long-term storage purpose. The proposed charge allocation framework and optimization technique are general and can be applied to any type of battery banks so far as we have accurate battery models. Intensive work has been conducted to explore accurate and easy-to-use battery models. The electrochemistry-based models [27], [28] are accurate but too complicated to use in system-level design and optimization. We thus rely on a circuit-based battery model with good accuracy [29], [30] as we formulate the charge allocation problem in a mathematical form. Fig. 5 demonstrates the model accuracy comparing the measured Li-ion battery terminal voltage with simulation results from the circuit model for a discharging process. We describe the general properties of all the battery banks in this section, and omit the bank index k for notational simplicity.
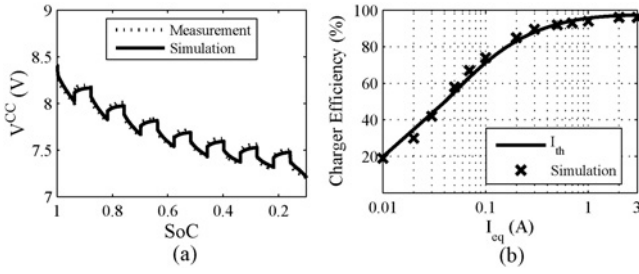
Fig. 5. (a) Comparison of the circuit model simulation results with the measured battery terminal voltage of two serial-connected 350 mAh Li-ion batteries. (b) Conversion efficiency of an LTM4607 power converter.

Fig. 4 shows a charging process of a Li-ion battery, with a runtime-based model on the left, and a circuit-based model on the right for accurately capturing of the battery service life and the I–V characteristics. In this model, the SoC is given by $SoC = C_b/C_{b,\text{full}}$. In practice, ignoring the battery aging, we derive $C_{b,\text{full}}$ from the nominal capacity (usually characterized in units of $A \cdot h$) of the battery. The battery OCV is modeled as a function depending on SoC. Other parameters, such as the internal resistance and capacitance, are functions of SoC as well. The functions are nonlinear and involve some empirical parameters b_{ij} [31]

$$
\begin{aligned}
V^{\text{OC}} &= b_{11}e^{b_{12} \cdot \text{SoC}} + b_{13}(\text{SoC})^3 + b_{14}(\text{SoC})^2 + b_{15}\text{SoC} + b_{16} \\
R_s &= b_{21}e^{b_{22} \cdot \text{SoC}} + b_{23}, \qquad R_{\text{ts}} = b_{31}e^{b_{32} \cdot \text{SoC}} + b_{33} \\
C_{\text{ts}} &= b_{41}e^{b_{42} \cdot \text{SoC}} + b_{43} \qquad R_{\text{tl}} = b_{51}e^{b_{52} \cdot \text{SoC}} + b_{53} \\
C_{\text{tl}} &= b_{61}e^{b_{62} \cdot \text{SoC}} + b_{63}.
\end{aligned} \tag{2}
$$

The rate capacity effect of batteries describes how the available charge in a battery relates to the magnitude of the discharging current [32]. Peukert's law is an empirical relation that accurately relates the discharging time and discharging current to the change of the battery charge. This law is described as $\Delta C_b = (I_{\text{array}})^{\gamma_d} \cdot t$, where t is the discharging time, and γ_d is the Peukert constant (1.05 and 1.3 depending on the battery type). A similar relationship can be approximately used for the charging process except that Peukert constant for charging γ_c is less than 1. Thus, we have

$$
\begin{aligned}
I_{\text{eq}} &= (I_{\text{array}})^{\gamma_c} \\
\text{SoC}(t) &= \text{SoC}(0) + \int_0^t \frac{(I_{\text{eq}}(\tau) - I_{\text{sd}}(\tau))}{C_{b,\text{full}}} \cdot d\tau
\end{aligned} \tag{3}
$$

where I_{eq} in (3) is the *equivalent charging current* inside the kth EES array, considering the rate capacity effect. The I_{eq} reflects the rate that a battery sends or receives charge. (3) shows that the I_{array} is a convex function of I_{eq}. Typically, I_{sd} is very small in batteries.

The OCV and CCV of a battery are generally not equal to each other. Fig. 4 shows that the difference between them is the voltage drop on the internal resistances R_s, R_{ts}, and R_{tl}

$$
V^{\text{CC}}(t) = V^{\text{OC}}(t) + V_{\text{tl}}(t) + V_{\text{ts}}(t) + I_{\text{array}}(t) \cdot R_s. \tag{4}
$$

3) *Supercapacitor Bank:* The supercapacitor is another representative EES element that has relatively lower energy density, but superior cycle efficiency and much longer cycle life compared to batteries. Thus, the supercapacitor banks are commonly used to deal with the peak power demand or
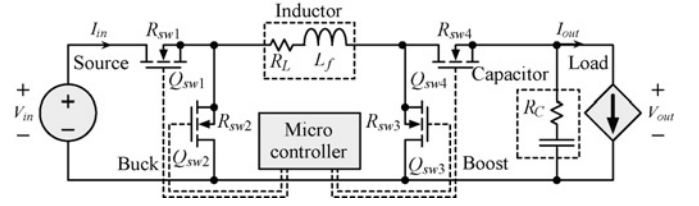

Fig. 6. Circuit model of the buck–boost converter.

supply. The rate capacity effect is negligible in supercapacitor and we have $I_{\text{array}} \approx I_{\text{eq}}$. The electrical circuit model for the supercapacitor used in this paper contains a low series resistance ($\sim$25 mΩ) [31]. Therefore, the following relation between $V^{\text{OC}}(t)$ and $V^{\text{CC}}(t)$ holds for the supercapacitors

$$
V^{\text{CC}}(t) = V^{\text{OC}}(t) + I_{\text{array}}(t) \cdot R_{\text{series}}. \tag{5}
$$

A fundamental disadvantage of the supercapacitor is the high self-discharge rate compared with other EES elements. A supercapacitor typically loses more than 20% of its stored energy per day due to self-discharge [33]. The voltage decay of a supercapacitor for a short time interval Δt is given by

$$
V^{\text{OC}}(t + \Delta t) = V^{\text{OC}}(t) \cdot e^{-\Delta t/\tau} \tag{6}
$$

where τ is the self-discharge time constant. Using Taylor expansion, the power loss rate due to self-discharge is given by

$$
P_{\text{sd}}(t) = C_{\text{cap}} \frac{\left(V_{\text{array}}^{\text{OC}}(t)\right)^2}{\tau}. \tag{7}
$$

4) *Charger:* We use a pulse width modulation (PWM) buck–boost converter model as the charger model. The input voltage, input current, output voltage, and output current of the charger are denoted by V_{in}, I_{in}, V_{out}, and I_{out}, respectively. A charger has two working modes: buck mode (if $V_{\text{in}} > V_{\text{out}}$) and boost mode otherwise. When the charger is turned ON, the power loss P_c of the charger consists of three components: conduction loss P_{cdct}, switching loss P_{sw}, and controller loss P_{ctrl}. The power loss of the charger is zero when the charger is turned OFF. Note that P_{sw} and P_{ctrl} are nonzero and not proportional to the output power. We adopt a binary indication variable x_c such that $x_c = 1$ if the charger is turned ON, and $x_c = 0$ otherwise. Thus, P_c is given by

$$
P_c = P_c^{\text{on}} \cdot x_c = (P_{\text{cdct}} + P_{\text{sw}} + P_{\text{ctrl}}) \cdot x_c. \tag{8}
$$

Fig. 6 shows a schematic of a PWM buck–boost converter. It consists of four switching MOSFETs whose ON–OFF states determine the operation mode of the converter. The power loss components are mainly determined by the PWM duty ratio D (less than 1), the maximum current ripple ΔI, the switching frequency f_s, the controller current $I_{\text{controller}}$, the equivalent series resistances R_L and R_C, and the turn-on resistance and gate charge of the ith MOSFET switch, R_{swi} and Q_{swi}. In the

buck mode, we adopt the power loss model in [34] as follows:

$$D = \frac{V_{\text{out}}}{V_{\text{in}}}, \qquad \Delta I = V_{\text{out}} \frac{1 - D}{L_f \cdot f_s}$$

$$P_{\text{cdct}} = I_{\text{out}}^2 \cdot (R_L + D \cdot R_{\text{sw1}} + (1 - D) \cdot R_{\text{sw2}} + R_{\text{sw4}})$$

$$+ \frac{(\Delta I)^2}{12} \cdot (R_L + D \cdot R_{\text{sw1}} + (1 - D) \cdot R_{\text{sw2}} + R_{\text{sw4}} + R_C)$$

$$P_{\text{sw}} = V_{\text{in}} \cdot f_s \cdot (Q_{\text{sw1}} + Q_{\text{sw2}})$$

$$P_{\text{ctrl}} = V_{\text{in}} \cdot I_{\text{controller}}. \tag{9}$$

Note that in (9), the switching loss P_{sw} and controller loss P_{ctrl} are independent of I_{out}. We derive the power loss in boost mode based on the power loss in buck mode

$$D = 1 - \frac{V_{\text{in}}}{V_{\text{out}}}, \qquad \Delta I = V_{\text{in}} \frac{D}{L_f \cdot f_s}$$

$$P_{\text{cdct}} =$$
$$(\frac{I_{\text{out}}}{1 - D})^2 \cdot (R_L + DR_{\text{sw3}} + (1 - D)R_{\text{sw4}} + R_{\text{sw1}} + D(1 - D)R_C)$$

$$+ \frac{(\Delta I)^2}{12} \cdot (R_L + D \cdot R_{\text{sw3}} + (1 - D) \cdot R_{\text{sw4}} + R_{\text{sw1}} + (1 - D) \cdot R_C)$$

$$P_{\text{sw}} = V_{\text{out}} \cdot f_s \cdot (Q_{\text{sw3}} + Q_{\text{sw4}})$$

$$P_{\text{ctrl}} = V_{\text{in}} \cdot I_{\text{controller}}. \tag{10}$$

We extract the model parameters based on LTM4607 [35] converter and compare the simulated and measured conversion efficiency in Fig. 5(a).

5) CTI: We assume that the CTI is an ideal conductor in this paper. The American wire gauge data show that AWG 1 wire has 0.4066 mΩ/m. As the typical wire length in an HEES system is in order of meters, the resistance is approximately ~ 1 mΩ, which is negligible compared to the internal resistance of the EES bank arrays (a single Li-ion battery usually has internal resistance of 0.1$\sim$0.2 Ω.) Furthermore, the CTI inductance is even more negligible because the CTI bus voltage changes very slowly. The CTI bus capacitance is orders of magnitude smaller than the bank array capacitance.

B. Charge Allocation Optimization Problem Formulation

In this paper, we target the charge allocation problem of an HEES system with an energy harvesting system, e.g., a PV module. Fig. 3 shows the diagram of the system. The PV module collects the solar energy and delivers the energy to the HEES system. The charge allocation process starts at time $t = 0$ and ends at time $t = T_a$. From the initial SoCs of all EES banks, we determine the OCV of EES arrays $V_{\text{array,k}}^{\text{OC}}(0)$ for all EES banks. We observe the solar radiation levels in the target area and based on this predict the power generation profile of the PV module over the charge allocation process.

The charge allocation process is managed by three sets of control variables that should be optimally determined for the highest global efficiency. The first one is CTI voltage $V_{\text{cti}}(t)$, which is maintained by the source-to-CTI charger. The second one is the set of selected EES banks, $S'(t) \in S$. The third set of variables is $\{I_{\text{array,k}}(t)\}, k \in S$ of all the EES banks, which are tuned by the EES bank chargers. Note that an array charging current can be set to 0, i.e., we turn off the charger if we decide not to charge that EES bank. The solution of the charge allocation problem consists of three parts: $V_{\text{cti}}(t)$, $S'(t)$,

and $\{I_{\text{array,k}}(t)\}, k \in S, t \in [0, T_a]$. We formulate the GCA as a mathematical programming problem, while the objective function is the GCA efficiency and variables are the three variables aforesaid.

We derive the constraints in the mathematical programming problem based on the law of energy conservation. Electrical energy is generated by PV and delivered to the CTI through the source-to-CTI charger, where it is further distributed by selected chargers to their corresponding destination EES banks. Based on the law of energy conservation, the power supplied by the power source $P_{\text{src}}(t)$ consists of $P_{c,s}(t)$, $P_{\text{waste}}(t)$ and the power delivered to CTI $P_{\text{cti}}(t)$; thus, the energy conservation for the CTI is given by

$$
\begin{aligned}
P_{\text{src}}(t) &= V_{\text{src}}(t) \cdot I_{\text{src}}(t) = P_{c,s}(t) + P_{\text{cti}}(t) + P_{\text{waste}}(t) \\
&= P_{c,s}(t) + V_{\text{cti}}(t) \sum_{k=1}^{N} I_{\text{bank,k}}(t) + P_{\text{waste}}(t). \quad (11)
\end{aligned}
$$

For the kth charger, the output power equals the input power minus the power loss during the conversion. Thus, the energy conservation for the charger is given by

$$
\begin{aligned}
V_{\text{cti}}(t) \cdot I_{\text{bank,k}}(t) &= V_{\text{array,k}}^{\text{CC}}(t) \cdot I_{\text{array,k}}(t) + P_{c,k}(t) \\
&= V_{\text{array,k}}^{\text{CC}}(t) \cdot \left(I_{\text{eq,k}}(t)\right)^{1/\gamma_c} + P_{c,k}(t). \quad (12)
\end{aligned}
$$

$P_{c,k}(t)$ and $P_{c,s}(t)$ in (11) and (12) can be derived using (8)–(10) but with different sets of parameters.

We define the objective function as the GCA efficiency, or equivalently, the total energy gain in all EES banks after the charge allocation process, i.e., the integration of the power pushed into all EES banks minus the leakage power as in (7). Continuing the previous analysis, the energy increase rate in the kth EES bank, denoted by $P_{\text{gain,k}}(t)$, is given by

$$P_{\text{gain,k}}(t) = V_{\text{array,k}}^{OC}(t) \cdot I_{\text{eq,k}}(t) - P_{\text{sd,k}}(t) \tag{13}$$

$$\frac{d}{dt} E_{\text{HEES}}(t) = \sum_{k=1}^{N} P_{\text{gain,k}}(t) \tag{14}$$

where the $E_{\text{HEES}}(t)$ is the the total energy stored in all HEES banks. Note that the first term on the right-hand side (RHS) in (13) corresponds to the power that is pushed into the kth EES bank. Compared to the first term on the RHS in (12), we exclude the power dissipation on the internal resistance of the EES banks and the power loss due to the rate capacity effect from the output power of the kth charger.

We formulate the GCA optimization problem as follows. **Given:** Initial SoCs of all destination EES banks, SoC(t)|$_{t=0}$, $\forall k \in S$; (historic) profile of the solar radiation; specifications of the HEES system and the PV module; and duration of the charge allocation process $[0, T_a]$.
Find: $V_{\text{cti}}(t)$, $S'(t)$, and $I_{\text{array,k}}(t)$, $\forall k \in S$ and $\forall t \in [0, T_a]$.
Maximize: the GCA efficiency η_{GCA}, which is given by

$$\eta_{\text{GCA}} = \frac{\sum_{k=1}^{N} \int_0^{T_a} P_{\text{gain,k}}(t) dt}{\int_0^{T_a} P_{\text{src}}(t) dt} \tag{15}$$

or equivalently maximize the total energy increment in all the destination EES banks at time T_a, given by the nominator term in (15), since the denominator term in (15) is fixed.

Subject to: 1) Lower and upper bound of the array charging currents

$$0 \leq I_{\text{eq,k}}(t) \leq I_{\text{max,k}}, \forall t \in [0, T_a], \forall k \in S. \quad (16)$$

2) Maximum energy storage constraint

$$E_k(0) + \int_0^t P_{\text{gain,k}}(\tau)d\tau \leq E_{\text{max,k}}, \forall t \in [0, T_a] \quad (17)$$

where $E_k(0)$ stands for the initial energy stored in the kth bank at the beginning of the charge allocation process.
3) The conservation of energy given by (11) and (12).
4) The conservation of charge given by (3).

Although $\{I_{\text{array,k}}(t)\}$ is the set of variables that we can control using the chargers, we use $\{I_{\text{eq,k}}(t)\}$ as the optimization variables instead in the formulation because of the convenience in solving the optimization problem. We determine $\{I_{\text{array,k}}(t)\}$ from solved $\{I_{\text{eq,k}}(t)\}$ according to (3). In addition, the GCA optimization problem is an MINLP problem due to the existence of binary variables $\{x_{c,k}(t)\}$. Therefore, the GCA optimization problem is NP-complete and cannot be optimally solved in polynomial time. We provide an approximation algorithm to obtain the near-optimal solution of the GCA problem.

IV. METHODOLOGY

Before solving the GCA problem, we first consider the ICA problem, which aims to optimize the charge allocation efficiency at a specific time instance. We present an algorithm to solve the ICA problem and derive a near-optimal solution. Subsequently, we break the whole charge allocation process into a series of time slots and solve one ICA problem at each decision epoch. However, a simple combination of the ICA solutions at each decision epoch is a greedy decision, which may not achieve the global optima due to the lack of consideration of SoC changes in the EES banks, especially those banks that have small energy capacity and high charging efficiency.[2] To overcome this issue, we incorporate an upper bound on the total charging power of the high-charging-efficiency banks.

The rest of this section is organized as follows. We first present the heuristic for predicting the solar power in Section IV-A. Then, we elaborate the near-optimal ICA solver and the heuristic for deriving the charging power limits in Sections IV-B and IV-C, respectively. Finally, we solve the GCA problem as a time series of solutions to the constrained ICA problems. Table III lists the important notations used in the following text.

A. Solar Irradiance Level Prediction

Accurate online solar irradiance forecast, which provides the clue of future power generation, is extremely important in developing the GCA algorithm since the optimal GCA policy depends on the power generation profile. We break the daily observation of solar irradiance level into M time slots

---

[2]We classify all EES banks into two groups: high-charging-efficiency banks (e.g., supercapacitor banks) and low-charging-efficiency banks (e.g., battery banks) according to their properties.

TABLE III
NOTATION USED IN SECTION IV

Notation	
d_n, t_m	at the t_mth time slot in the d_nth day
$C_s(d_n, t_m)$	clear sky solar irradiance level (W/m²)
$R_s(d_n, t_m)$	observed solar irradiance level (W/m²)
$\xi_c(d_n, t_m)$	climate condition factor, typically less than 1
$\gamma(t_m)$	screening factor to judge whether the solar irradiance is affected by the climate conditions
$Pd_s(d_n, t_m)$	predicted solar irradiance level (W/m²)
$P_{\text{SB}}^{\text{up}}(t_m)$	upper limit for the charging power of all supercapacitor banks
E_{SB}	the energy stored in all supercapacitor banks
E_{BB}	the energy stored in all battery banks

$(0, t_1, t_2, ..., t_M)$. We consider two factors in order to accurately predict the solar irradiance: clear sky solar irradiance level $C_s(d_n, t_m)$ (i.e., solar irradiance in a sunny day), which stands for the maximum solar irradiance level without any decay due to the climate conditions, and climate condition factor $\xi_c(d_n, t_m)$, which takes into account the decay factor caused by climate conditions, such as rain, cloud, and so on. We set each time slot to be 10–15 min so that the solar irradiance level and climate conditions are approximately unchanged within a time slot.

We consider that the climate conditions have an approximately linear decaying effect on the solar irradiance levels. To obtain the *predicted solar irradiance level* $Pd_s(d_n, t_m)$, we multiply the climate condition factor at previous time instance $\xi_c(d_n, t_{m-1})$ to $C_s(d_n, t_m)$. At the end of the t_mth time instance, we observe the solar irradiance level $R_s(d_n, t_m)$ and calculate $\xi_c(d_n, t_m)$ as relative ratio between $R_s(d_n, t_m)$ and $C_s(d_n, t_m)$

$$Pd_s(d_n, t_m) = C_s(d_n, t_m) \cdot \xi_c(d_n, t_{m-1})$$
$$\xi_c(d_n, t_m) = \frac{R_s(d_n, t_m)}{C_s(d_n, t_m)}. \quad (18)$$

Although $C_s(d_n, t_m)$ varies with the location on the earth and the time of the year, it is predictable based on the observation history of solar irradiance levels [36]. We adopt exponential smoothing, which is a powerful technique that is applied to sequential data to make forecasts by assigning exponentially decreasing weights over time [6]. This weighting method makes exponential smoothing particularly effective in our problem since $C_s(d_n, t_m)$ is more related to the solar irradiance in recent past rather than earlier past. We observe $R_s(d_n, t_m)$ and update $C_s(d_n, t_m)$ using a smoothing factor α, which ranges between 0 and 1. The $C_s(d_n, t_m)$ is given by

$$C_s(d_1, t_m) = 0,$$
$$C_s(d_{n+1}, t_m) = C_s(d_n, t_m), \text{ if } R_s(d_n, t_m) < \lambda(t_m)C_s(d_n, t_m)$$
$$C_s(d_{n+1}, t_m) = \alpha \cdot C_s(d_n, t_m) + (1-\alpha) \cdot R_s(d_n, t_m), \text{ otherwise.}$$
$$(19)$$

Since $C_s(d_n, t_m)$ denotes the clear sky solar irradiance level, we use $\lambda(t_m)$ as a *screening factor* to prune the solar irradiance data that severely degrade due to the climate conditions in (19) and only update $C_s(d_n, t_m)$ using those data that are collected in sunny days. More precisely, if $R_s(d_n, t_m) < \lambda(t_m) \cdot C_s(d_n, t_m)$, we consider it to be not under clear sky condition, and thereby directly carry $C_s(d_n, t_m)$ to the next time instance. We determine $\lambda(t_m)$ based on an online learning approach,

where the *state set* is defined as the set of time slots $\{t_m\}$, the *action set* is defined as a set of different reasonable screening factors $(\lambda_1, \lambda_2, ..., \lambda_K)$ (i.e., 0.7–1). Selecting different λ_k ends up with different $C_s(d_{n+1}, t_m)$ and in turn affects the predictions later on. The prediction error is captured by the *penalty function Error_m*. We adopt Q-learning and update the state–action pair $Q(t_m, \lambda_k)$ using a learning rate β

$$\text{Error}_m = |Pd_s(d_n, t_m) - R_s(d_n, t_m)|$$
$$Q(t_m, \lambda_k) \leftarrow (1 - \beta) \cdot Q(t_m, \lambda_k) + \beta \cdot \text{Error}_m. \quad (20)$$

We pick the screening factor λ_k according to the probability of $\dfrac{\exp(-Q(t_m, \lambda_k))}{\sum_{k=1}^{K} \exp(-Q(t_m, \lambda_k))}$.

B. ICA Solver

The ICA optimization problem maximizes the total power that is pushed into all EES banks at a specific time instance. The ICA problem is a special case of the GCA problem when $T_a \rightarrow 0$. The control variables to be solved in the ICA problem are similar to GCA problem, except that they are only for one time instance. Thus, we omit t for simplicity in writing. We define the objective function *ICA efficiency* η_{ICA} as

$$\eta_{\text{ICA}} = \frac{1}{P_{\text{src}}} \sum_{k=1}^{N} P_{\text{gain},k} \quad (21)$$

where the P_{src} is a fixed value and do not affect the optimization. We apply similar constraints (11) and (12) to the ICA problem. Therefore, the ICA optimization problem is again an MINLP problem. We utilize three facts to simplify the original ICA problem to *optimal charging current determination* (OCCD) problem, which is a convex optimization problem. The three facts are as follows.

1) The optimal ICA efficiency η_{ICA} is approximately an unimodal function with respect to the CTI voltage V_{cti}. Therefore, we perform a ternary search[3] in the feasible region of V_{cti} as the outer loop. Inside the outer loop, we consider the CTI voltage V_{cti} as a fixed value and solve the OCCD problem. More precisely, we do not treat V_{cti} as an variable in OCCD problem; otherwise, solving the $\{I_{\text{eq},k}\}$ becomes impractical because the power loss in the charger (8)–(10) is a function of both $\{I_{\text{eq},k}\}$ and the CTI voltage.

2) It will be beneficial to turn off some EES banks if their optimal $\{I_{\text{eq},k}\}$ are smaller than a threshold value I_{th}. The charger power loss contains a fixed part and a part proportional to the output charging current. It is not worthwhile to keep the charger ON when the output charging current is small. The binary indicators $\{x_{c,k}\}$ that denote the charger status lead to the discontinuity in optimization problem. To overcome this issue, we maintain a selection set S', which is a subset of S, and only consider $I_{\text{eq},k}, k \in S'$ in the OCCD problem, i.e., $x_{c,k} = 1, k \in S'$. For other EES banks that are not in S', we set $I_{\text{eq},k} = 0, x_{c,k} = 0, k \notin S'$. In this way, the OCCD problem becomes a continuous mathematical programming problem.

---

[3]A ternary search is a divide and conquer-based algorithm that determines either that the minimum or maximum cannot be in the first third of the domain or that it cannot be in the last third of the domain, then repeats on the remaining two-thirds.

Algorithm 1: ICA solver (ICAS)

Input: The initial SoC_k, $\forall k \in S$, the input power P_{src} and V_{src}, the feasible region of CTI voltage $(V_{\text{cti,min}}, V_{\text{cti,max}})$, and predefined parameters ϵ, I_{th}, ΔV_{th}.

1   Determine the OCVs $V_{\text{array},k}^{\text{OC}}$, $\forall k \in S$ based on SoCs;
2   **repeat**
3   **for** $V_{\text{cti}}^{(1)} = \frac{1}{3} V_{\text{cti,min}} + \frac{2}{3} V_{\text{cti, max}}$, *and* $V_{\text{cti}}^{(2)} = \frac{2}{3} V_{\text{cti, min}} + \frac{1}{3} V_{\text{cti,max}}$, **do**
4       $i \leftarrow 0$;
5   Initialize $S'^{(0)} \leftarrow S$;
6   Initialize $V_{\text{array},k}^{\text{CC},(0)} \leftarrow V_{\text{array},k}^{\text{OC}}$, $\forall k \in S'^{(0)}$;
7   **repeat**
8         $i \leftarrow i + 1$, $S'^{(i)} \leftarrow S'^{(i-1)}$;
9   Solve the OCCD problem with fixed V_{cti}, $S'^{(i-1)}$ and $V_{\text{array},k}^{\text{CC},(i-1)}$, $\forall k \in S'^{(i-1)}$, find the optimal $\{I_{\text{eq},k}^{(i)}, k \in S'^{(i-1)}\}$;
10         $\forall k \in S'^{(i-1)}$, **if** $I_{\text{eq},k}^{(i)} < I_{\text{th}}$, **then**
11           $I_{\text{eq, }k}^{(i)} \leftarrow 0$ and $S'^{(i)} \leftarrow S'^{(i)} \backslash k$
12   Calculate $\{I_{\text{array},k}^{(i)}$, update $V_{\text{array},k}^{\text{CC}, (i)}$, $\forall k \in S'^{(i)}$ using (3)–(5)
13   **until** $\max_{k \in S'^{(i)}} \left| V_{\text{array},k}^{\text{CC}, (i)} - V_{\text{array},k}^{\text{CC},(i-1)} \right| < \epsilon$ *and* $S'^{(i)} = S'^{(i-1)}$;
14   Calculate $\eta_{\text{ICA}}(V_{\text{cti}})$, using (21);
15   **if** $\eta_{\text{ICA}}\left(V_{\text{cti}}^{(1)}\right) < \eta_{\text{ICA}}\left(V_{\text{cti}}^{(2)}\right)$, **then**
16       $V_{\text{cti,min}} \leftarrow \frac{1}{3} V_{\text{cti,min}} + \frac{2}{3} V_{\text{cti,max}}$
17   **else**
18       $V_{\text{cti,max}} \leftarrow \frac{2}{3} V_{\text{cti,min}} + \frac{1}{3} \cdot V_{\text{cti,max}}$
19   **until** $|V_{\text{cti,max}} - V_{\text{cti,min}}| < \Delta V_{\text{th}}$;
20   $V_{\text{cti}} \leftarrow \frac{1}{2}(V_{\text{cti,min}} + V_{\text{cti,max}})$
21   **return** V_{cti}, $S'^{(i)}$, and $I_{\text{eq},k}^{(i)}$, $\forall k \in S$

For each fixed V_{cti}, we first initialize S' to be the full set of all EES banks and remove those EES banks whose $I_{\text{eq},k}$ is smaller than I_{th}. We repeat solving the OCCD problem until the selection set S' converge.

3) In general, the CCVs are not very different from OCVs since the internal resistances are not large, according to (4) and (5). The objective function is a complicated nonlinear function of $\{I_{\text{eq},k}\}$ since both the CCVs and $\{I_{\text{array},k}\}$ are involved in the charger's power loss. To address this issue, we use fixed CCVs $\{V_{\text{array},k}^{CC}\}$ in the OCCD problem instead of functions of $\{I_{\text{array},k}\}$. After solving the OCCD, we obtain the $\{I_{\text{eq},k}\}$ and update $V_{\text{array},k}^{CC}$ using (3)–(5). We repeat solving the OCCD problem until the $V_{\text{array},k}^{CC}$, $\forall k \in S'$ converge.

The proposed ICAS algorithm is summarized in Algorithm 1. We do ternary search of V_{cti} in the outer loop, while in the inner loop, we solve the OCCD problem repeatedly at a fixed V_{cti} and update the selection set S' as well as the CCV voltages $\{V_{\text{array},k}^{\text{CC}}\}$. The OCCD problem has a concave objective function (21) to be maximized, subjecting to linear inequality constraints (16) and convex inequality constraints (11) and (12). Thus, the OCCD problem is a convex optimization problem and can be solved optimally in polynomial time using the standard convex optimization technique. We carefully set the threshold current I_{th} such that turning OFF the charger when the $I_{\text{eq},k} < I_{\text{th}}$ always improves the charge allocation efficiency. Fig. 5(b) shows that when $I_{\text{eq},k} < 0.05$ A, the conversion efficiency of the charger becomes unacceptably low. Thus, we set I_{th} to be 0.05 A. The inner loop in Algorithm 1 is terminated when S' and $\{V_{\text{array},k}^{\text{CC}}\}$ converge, where the optimal η_{ICA} at a specific V_{cti} is achieved. We search the V_{cti} domain and repeat the inner loop subroutine for different V_{cti} until a termination condition is met, i.e., the difference between the upper and lower bounds of the V_{cti} domain falls within a predefined threshold ΔV_{th}.
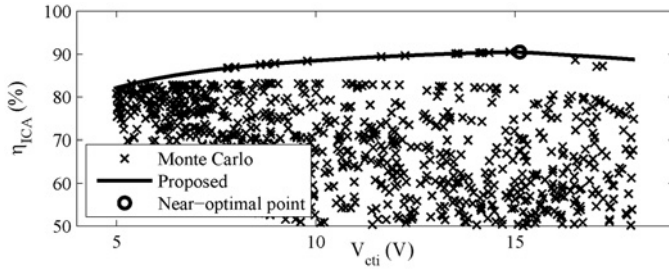
Fig. 7. Comparison of ICA efficiency η_{ICA} at different CTI voltages V_{cti} obtained by the proposed method (solid curve) and MC simulation (cross marks).

Fig. 7 shows η_{ICA} versus the V_{cti} for a four-bank HEES system. The solid curve shows that the η_{ICA} solved at each fixed V_{cti} is an unimodal function of V_{cti}. Thus, we converge to the near-optimal solution (displayed as a circle) by ternary searching the V_{cti} domain. The empty space in Fig. 7 below the solid curved is caused by the discontinuity of the $\{x_{c,k}\}$. The Monte Carlo (MC) simulation results (displayed as cross marks) shows that the proposed method always achieves better solutions than the MC simulation.

C. Power Limit Derivation

The ICAS algorithm presented in Section IV-B solves the ICA problems near-optimally and returns the corresponding EES bank selection, CTI voltage, and EES array charging currents. A straightforward way to solve the GCA problem is to follow a greedy approach, i.e., breaking the whole charge allocation process into a series of consecutive time slots $(0, t_1, t_2, ..., t_M)$ and solving an ICA problem at the beginning of each time slot, with the approximation that the SoC stays unchanged over the time slot. However, such an greedy approach does not consider the EES bank capacity, and thereby may not lead to the optimal results, e.g., simply assigning a large amount of power to high-charging-efficiency banks. As shown in Fig. 1, supercapacitor banks usually have high charging efficiency thanks to their high power capacity and small internal resistance, while their energy capacity is very limited. Therefore, the greedy GCA approach may fully charge the supercapacitor banks very quickly and then assign all power to battery banks during the rest of the charge allocation process. In such a case, the GCA efficiency may be unacceptably low due to the following two reasons.

1) The power loss due to the rate capacity effect in the battery banks increases superlinearly as the array charging current increases, according to Peukert's law. The greedy approach may charge the battery banks with high rates after all supercapacitor banks are full. Thus, the HEES system suffers a significant power loss that prevents it from reaching the global optimality.

2) The other reason that makes the greedy approach even worse is the self-discharge of the supercapacitor banks. The self-discharge power rate grows quadratically as the OCV of the supercapacitor bank increases, according to (7). Thus, the high leakage rate degrades the GCA efficiency if we charge the supercapacitor banks quickly and leave them at high SoC state for the rest of charge allocation process.

Due to these reasons, we modify the original ICAS to make it aware of the future energy generation. More precisely, we impose an upper limit for the total charging power of all the supercapacitor banks, $P_{\text{SB}}^{\text{up}}(t_m)$, to prevent rapid charging of supercapacitor banks, leaving some capacity for the remaining charge allocation process to combat the rate capacity effect and alleviate the power loss due to the self-discharge. A low power limit may undercharge the supercapacitor banks and result in low GCA efficiency, since the supercapacitor banks typically have high charging efficiency. Furthermore, the power limit should also consider the power generation. For example, the power limit should be relatively high during the peak period of the power supply in order to allow more power to be assigned to the supercapacitor banks. An effective heuristic of setting the appropriate power limits to achieve the near-optimal GCA efficiency is to charge the supercapacitor banks such that they are fully charged at the end of the charge allocation process.

Since supercapacitor banks typically have higher charging efficiency, the ICAS intends to assign full $P_{\text{SB}}^{\text{up}}(t_m)$ amount of power to them. Therefore, the energy assigned to all supercapacitor banks (E_{SB}) and battery banks (E_{BB}) over the whole charge allocation process are approximately given by

$$E_{\text{SB}} = \sum_{m=1}^{M} \int_{t_{m-1}}^{t_m} P_{\text{SB}}^{\text{up}}(t_m) dt,$$

$$E_{\text{BB}} = \sum_{m=1}^{M} \int_{t_{m-1}}^{t_m} \left(P_{\text{src}}(t_m) - P_{\text{SB}}^{\text{up}}(t_m) \right) dt. \tag{22}$$

According to (6) and (7), we conclude that the ratio between energy loss due to self-discharge and the total energy is fixed and given by $\mu_{\text{sd}} = E_{\text{SB}}(t + \Delta t)/E_{\text{SB}}(t) = e^{-2\Delta t/\tau}$, where Δt is the duration of a time slot and $\mu_{\text{sd}} < 1$ is the ratio of remaining energy after one time slot. Therefore, the total energy loss due to the self-discharge E_{sd} is approximately given by

$$E_{\text{sd}} = E_{\text{SB}} - \sum_{m=1}^{M} \int_{t_{m-1}}^{t_m} (1 - \mu_{\text{sd}})^{(M-m+1)} P_{\text{SB}}^{\text{up}}(t_m) dt. \tag{23}$$

We denote the part of the energy assigned to all the battery banks but wasted due to the rate capacity effect by E_{rb}. For derivation simplicity, we approximately treat all battery banks as a big equivalent battery with an equivalent Peukert constant $\gamma_{\text{eq}} < 1$. Thus, E_{rb} is given by

$$E_{\text{rb}} = E_{\text{BB}} - \sum_{m=1}^{M} \int_{t_{m-1}}^{t_m} \left(P_{\text{src}}(t_m) - P_{\text{SB}}^{\text{up}}(t_m) \right)^{\gamma_{\text{eq}}} dt. \tag{24}$$

We determine the parameter γ_{eq} in (24) by fitting the energy loss due to rate capacity effect of all battery banks. The power limit is constrained by the energy capacity of all the supercapacitor banks. This helps us to express the energy loss due to the self-discharge and rate capacity effect as convex functions of $\{P_{\text{SB}}^{\text{up}}(t_m)\}$. The derivation of power limit becomes an optimization problem as follows:

Minimize: $E_{\text{rb}} + E_{\text{sd}}$, $\tag{25}$

Subject to: maximum energy constraint for SB,

$$\sum_{m=1}^{M} \int_{t_{m-1}}^{t_m} P_{\text{SB}}^{\text{up}}(t_m) dt \leq \frac{1}{2} \sum_{k \in \text{SB}} C_{\text{cap,k}} \cdot (V_{\text{max,k}}^2 - (V_{\text{array,k}}^{\text{OC}})^2) \tag{26}$$

where $V_{\mathrm{max,k}}$ is the maximum voltage of the supercapacitor bank and $V_{\mathrm{array,k}}^{\mathrm{OC}}$ is the current OCVs. Equation (25) is a convex function and (26) is a linear constraint. Thus, we solve the optimization problem (25) using Lagrange multiplier and achieve the optimal set of $\{P_{\mathrm{SB}}^{\mathrm{up}}(t_m)\}$ over all time slots. The source power information that is required in (22)–(25) comes from the solar irradiance level prediction in Section IV-A. The power upper limit may change due to the variation of the climate condition. We determine this limit at every time slot according to the latest information of climate conditions and remaining capacity of the supercapacitor banks.

D. GCA Solver

In this section, we present the *GCA solver with charging power limits* (SCPL) for the GCA problem, integrating solar irradiance level prediction, power limits derivation, and modified ICAS alternately. The original ICAS finds the near-optimal solution of the ICA problem by iteratively solving OCCD problem and updating the CCVs and EES banks selection set. We modify the original ICA problem to constrained ICA problem by introducing a new constraint for the supercapacitor banks as follows:

$$V_{\mathrm{cti}}(t) \cdot \sum_{k \in \mathrm{SB}} I_{\mathrm{bank,k}}(t) \leq P_{\mathrm{SB}}^{\mathrm{up}}(t_m), \forall t \in [t_{m-1}, t_m]. \quad (27)$$

Since (27) is a convex inequality constraint, the OCCD in constrained ICA problem is still a convex optimization problem. We propose the SCPL algorithm as follows. We first break the whole charge allocation process into a series of short time slots $(0, t_1, t_2, ..., t_M)$. For each time slot, we observe the current solar irradiance level, make prediction of the solar irradiance level over the rest time of the day, derive the power upper limits for the supercapacitor banks, and solve the constrained ICA problem. The SCPL algorithm is summarized as Algorithm 2. The SCPL algorithm solves the GCA problems and derives the CTI voltage setting $V_{\mathrm{cti}}(t)$, selected set of the EES banks $S'(t)$, and the array charging currents $\{I_{\mathrm{array,k}}(t)\}$ for the selected EES banks over the whole charge allocation process. Our claim that the proposed algorithm returns a near-optimal solution of the GCA problem is based on the above flow in which each subproblem is solved near-optimally.

E. Temperature, Aging, and Malfunction Handling

The optimal management policy of the HEES should account for the effect of temperature. Intensive research has been conducted to study the battery behaviors at various temperatures. It turns that the cycling capacity, i.e., battery charge $C_{b,\mathrm{full}}$, only varies slightly (less than 5%) from 25 °C to 60 °C [37], [38]. The internal resistance of the battery does not vary much ($\sim$ 10%) either with the temperature rising [37]. Therefore, we ignore the temperature effect in the proposed SCPL algorithm. The GCA problem only solves the allocation problem for one charging process and does not involve cycling.

The batteries age as the HEES system is being operated, which causes capacity fading and the increase of internal resistance. Some known factors, such as the depth of discharge and average SoC significantly affect the battery aging. Thus,

---

Algorithm 2: GCA solver with charging power limits (SCPL)

Input: The specifications of the HEES system and PV module; initial SoC_k, $\forall k \in S$; duration of charge allocation process $[0, T_a]$ on the d_nth day; observation history of previous solar irradiance level, $C_s(d_{n-1}, t_m)$, $m \in [1, 2, ..., M]$.

1   Break $[0, T_a]$ into M time slots $(0, t_1, t_2, ..., t_M)$;
2   **for** $(m \leftarrow 1; m \leq M; m++)$ **do**
3   Observe $R_s(d_n, t_m)$;
4   Update $C_s(d_n, t_m)$ using (19) and (20);
5   Calculate $\xi_c(d_n, t_m) \leftarrow \frac{R_s(d_n, t_m)}{C_s(d_n, t_m)}$
6   Predict $Pd_s(d_n, t_k), \forall k > m$, using (18);
7   Calculate the remaining capacity in supercapacitor banks;
8   Derive the $P_{\mathrm{SB}}^{\mathrm{up}}(t_m)$ according to remaining capacity in supercapacitor banks and $Pd_s(d_n, t_k), m < k \leq M$, using (22)–(25);
9   Perform modified ICAS with power limit $P_{\mathrm{SB}}^{\mathrm{up}}(t_m)$ and find $V_{\mathrm{cti}}(t)$, $S'(t)$, and $I_{\mathrm{eq,k}}(t), \forall k \in S, t \in [t_{m-1}, t_m]$;
10   Calculate $I_{\mathrm{array,k}}(t)$ based on $I_{\mathrm{eq,k}}(t), \forall k \in S$;
11   Update SoCs and OCVs of all EES banks, using (2) and (3);
12   **return** $V_{\mathrm{cti}}(t)$, $S'(t)$, and $I_{\mathrm{array,k}}(t), \forall k \in S, t \in [0, T_a]$

---

we perform Coulomb counting for each EES bank, calculate the state of health (SoH) degradation, and update model parameters according to the SoH degradation. In fact, a high temperature significantly speeds up the battery aging. We record the battery temperature so that we can accurately update the characteristics of the aged battery including the battery capacity and internal resistances [39], [40].

In practice, a part of EES elements may have malfunction during runtime. We address this issue at the bank level and system level. A more elaborated dynamic bank reconfiguration [11] improves fine-granularity fault tolerance of the EES bank, which is a bank-level method. We simply exclude the unavailable banks from the set of available EES banks at the system level. We update bank set S at the beginning of each decision epoch and perform the proposed method because the GCA problem is solved in a discrete time manner.

V. SIMULATION RESULTS

We consider two different HEES systems: one consists of four EES banks (two supercapacitor banks and two battery banks), and the other consists of eight EES banks (four supercapacitor banks and four battery banks.) We use the solar irradiance level data that are collected in Los Angeles for year 2011 [25] and use PV modules with MPTT technique [24] as the power source. We consider the charge allocation process lasting for 12 h and solve corresponding GCA problems using the proposed GCA algorithm for both HEES systems. We extract the model parameters of chargers, Li-ion batteries, and supercapacitors through real measurements based on the Linear Technology LTM4607 converter [35], the GP1051L35 Li-ion battery cells [41], and the Maxwell BCAP P270 series supercapacitor [42].

The baseline setups in the simulation include: 1) unbiased bank charging (UB), the input power is uniformly allocated into all EES banks; 2) battery banks first policy (BBF), the input power is allocated into all battery banks; and 3) supercapacitor banks first scheme (SBF), the input power is allocated into all supercapacitor banks. The BBF policy ignores the supercapacitor banks and is used to mimic the homogeneous battery-only EES systems. Note that the SBF policy switches to BBF if all supercapacitor banks are fully
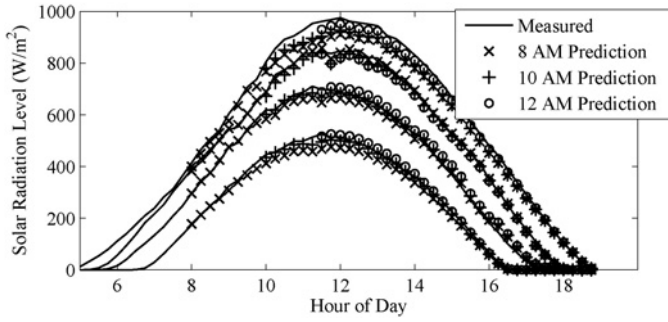
Fig. 8. Outcomes of the proposed solar irradiance level predictor at 8 AM, 10 AM, and 12 AM. The four groups from top to bottom are the average solar irradiance levels for July, April, September, and December, respectively.
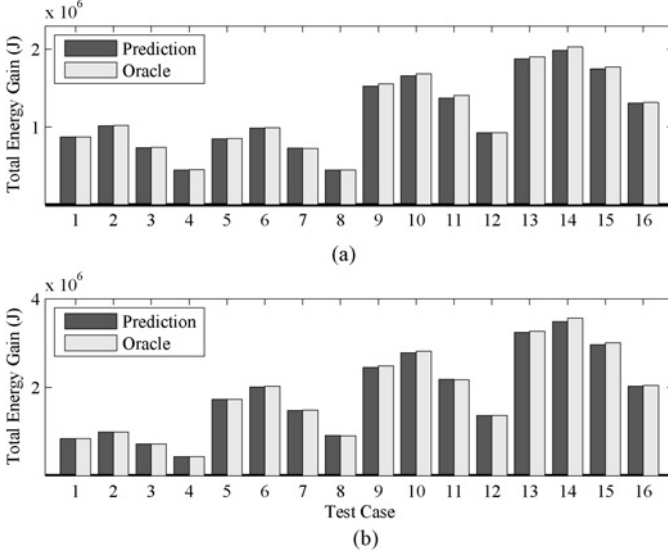

Fig. 9. Comparisons of the GCA with the proposed solar prediction method and Oracle system for (a) four-bank HEES system and (b) eight-bank HEES system.

charged. We use a constant CTI voltage for the baseline setups during the whole charge allocation process. We operate the baseline systems at several representative CTI voltage values and compare the results with that of the proposed SCPL algorithm. We investigate different solar irradiance levels in a year (April, July, September, and December) and PV module configurations[4] (4×2, 2×4, 4×4, 4×6 for four-bank HEES system and 4×2, 4×4, 4×6, 6×6 for eight-bank HEES system), with 16 test cases in total for each HEES system.

A. Solar Irradiance Level Prediction

Fig. 8 shows the monthly average solar irradiance level prediction using the proposed online prediction method at three time instances: 8 AM, 10 AM, and 12 AM in April, July, September, and December. We predict the solar irradiance level for the remaining charge allocation process at each time instance. The average error of the proposed prediction heuristic is less than 10%.

Fig. 9 compares the total energy gain in HEES systems for all the 16 test cases between the SCPL algorithm using

[4]For a PV module with configuration of $n \times m$, n and m denote the number of series- and parallel-connected PV cells, respectively.
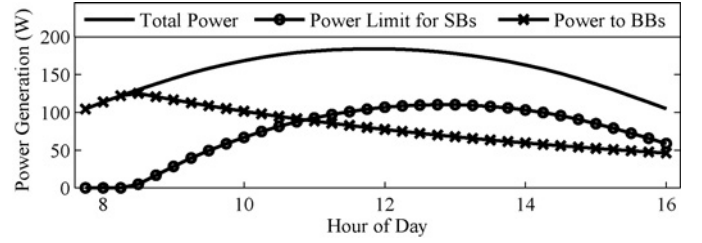

Fig. 10. Power limit for supercapacitor banks (SBs) that is derived from the proposed heuristic. The data are generated using the eight-bank HEES system with the 4×6 PV module. Simulated using solar data in Los Angeles in July.

proposed solar irradiance prediction and the SCPL algorithm using Oracle system.[5] The results in Fig. 9 show that the performance degradation of the proposed SCPL algorithm due to the misprediction is within 2%.

B. Power Limit Derivation

Fig. 10 shows the power limit that is derived from the proposed heuristic for the eight-bank HEES system and 4×6 PV module, using solar irradiance data in July. The line with circle marks is the power limits of the supercapacitor banks and the line with cross marks is the power that is allocated to the battery banks. We use the supercapacitor banks to shave the peak of the power generation profile in order to alleviate the energy loss due to rate capacity effect. Although the average duration with effective solar irradiance is about 12 h, we only use the supercapacitor banks from about 8 AM to 4 PM, depending on the predicted solar irradiance level and when the power generation peak happens. Since the self-discharge rate is larger when the supercapacitor banks have higher SoCs, the proposed heuristic tends to assign more energy to supercapacitor banks in later part of the charge allocation process. Therefore, the line with cross mark has negative slope as shown in Fig. 10. The value of power limit depends on the relative magnitude between power generation rate, capacities of battery banks and supercapacitor banks.

C. GCA Problem

We set the initial OCVs of battery banks and supercapacitor banks as 7.4 and 3.0 V, respectively, for the four-bank HEES system. The eight-bank HEES system has the initial OCVs of battery banks of 7.4, 7.4, 3.7, and 3.7 V, respectively, and a 3.0 V initial OCVs for all the supercapacitor banks. The battery banks have large enough capacity to accommodate all the energy generated from the PV modules, while the supercapacitor banks do not. Although the PV configuration is known, the power generated in PV module is not fixed but depends on V_{cti} in our problem setup since we apply MPTT. Therefore, to have fair comparisons, we use total energy gain after the charge allocation process as the measure of solution quality, i.e., the nominator in (15). We normalize the total energy gain of the baseline systems to the results of the proposed SCPL algorithm in Tables IV and V.

[5]The Oracle system has the perfect knowledge of the solar irradiance over the remaining charge allocation process

TABLE IV

COMPARISON OF NORMALIZED GCA RESULTS AFTER A 12 H CHARGE ALLOCATION PROCESS FOR THE FOUR-BANK HEES SYSTEM

Case	$n \times m$	Month	SCPL	Baseline								
				UB			SBF			BBF		
				5 V	8 V	12 V	5 V	8 V	12 V	5 V	8 V	12 V
1		Apr	100.0%	84.7%	89.3%	88.5%	82.1%	92.1%	95.7%	65.0%	68.7%	68.4%
2		Jul	100.0%	83.1%	88.7%	88.8%	80.8%	91.9%	95.0%	61.6%	65.9%	65.8%
3	4×2	Sep	100.0%	87.9%	91.8%	90.1%	85.1%	94.3%	97.1%	69.8%	73.2%	72.6%
4		Dec	100.0%	92.8%	94.4%	89.9%	89.9%	96.7%	96.9%	79.1%	81.4%	80.0%
5		Apr	100.0%	87.5%	92.3%	89.1%	84.9%	95.2%	96.3%	67.1%	71.0%	69.4%
6		Jul	100.0%	85.6%	91.4%	88.9%	83.3%	94.4%	95.6%	63.4%	67.8%	66.4%
7	2×4	Sep	100.0%	89.3%	93.3%	89.3%	86.4%	95.8%	96.3%	70.8%	74.3%	72.5%
8		Dec	100.0%	93.6%	95.3%	88.9%	90.6%	97.7%	96.0%	79.7%	82.0%	79.5%
9		Apr	100.0%	82.8%	92.4%	95.1%	74.7%	83.5%	86.5%	53.8%	61.2%	60.4%
10		Jul	100.0%	85.4%	96.4%	98.5%	71.8%	81.4%	83.8%	53.6%	62.0%	61.3%
11	4×4	Sep	100.0%	82.0%	90.3%	92.3%	77.9%	86.4%	88.2%	55.1%	61.7%	61.1%
12		Dec	100.0%	81.7%	87.4%	87.4%	80.3%	91.5%	95.9%	58.7%	63.0%	63.0%
13		Apr	100.0%	88.1%	95.8%	97.3%	71.1%	81.6%	82.5%	52.3%	61.5%	61.5%
14		Jul	100.0%	86.7%	94.7%	96.6%	69.2%	79.4%	82.3%	53.2%	63.2%	63.8%
15	4×6	Sep	100.0%	86.0%	96.6%	98.8%	72.6%	82.5%	85.4%	52.4%	60.9%	60.5%
16		Dec	100.0%	78.6%	87.0%	89.0%	77.9%	87.1%	89.4%	51.2%	57.7%	57.0%

TABLE V

COMPARISON OF NORMALIZED GCA RESULTS AFTER A 12 H CHARGE ALLOCATION PROCESS FOR THE EIGHT-BANK HEES SYSTEM

Case	$n \times m$	Month	SCPL	Baseline								
				UB			SBF			BBF		
				5 V	8 V	12 V	5 V	8 V	12 V	5 V	8 V	12 V
1		Apr	100.0%	91.0%	92.7%	86.9%	88.5%	95.5%	95.6%	83.7%	86.1%	84.3%
2		Jul	100.0%	90.1%	93.1%	88.8%	86.6%	94.9%	96.2%	80.5%	83.1%	81.9%
3	4×2	Sep	100.0%	91.5%	92.1%	84.5%	89.7%	95.8%	94.7%	87.1%	88.8%	86.3%
4		Dec	100.0%	92.1%	88.5%	76.3%	92.9%	96.0%	91.2%	93.7%	93.8%	89.1%
5		Apr	100.0%	82.3%	88.7%	88.8%	79.3%	91.4%	96.1%	63.9%	68.6%	68.8%
6		Jul	100.0%	80.4%	87.9%	89.0%	78.2%	91.1%	95.9%	60.5%	65.7%	66.2%
7	4×4	Sep	100.0%	84.5%	90.1%	89.2%	81.6%	92.4%	96.2%	67.8%	72.1%	72.0%
8		Dec	100.0%	88.9%	92.1%	88.1%	86.0%	94.3%	95.2%	76.3%	79.5%	78.6%
9		Apr	100.0%	79.1%	88.4%	90.9%	77.4%	87.8%	91.5%	56.0%	62.1%	62.8%
10		Jul	100.0%	78.2%	88.8%	92.3%	73.4%	79.7%	81.7%	53.7%	61.3%	61.3%
11	4×6	Sep	100.0%	79.1%	87.2%	88.9%	77.4%	90.4%	95.2%	57.8%	63.3%	63.9%
12		Dec	100.0%	84.4%	90.3%	89.6%	81.9%	93.2%	96.9%	65.8%	70.3%	70.4%
13		Apr	100.0%	79.3%	92.2%	97.2%	71.0%	81.2%	84.3%	51.3%	60.1%	60.1%
14		Jul	100.0%	82.0%	94.6%	97.7%	68.4%	82.3%	85.4%	51.4%	61.1%	61.4%
15	6×6	Sep	100.0%	77.9%	89.3%	93.3%	73.0%	83.4%	87.1%	51.9%	60.3%	59.9%
16		Dec	100.0%	77.7%	86.1%	87.9%	76.6%	90.7%	97.3%	55.2%	60.7%	61.5%

Tables IV and V summarize the GCA results of the proposed SCPL algorithm and the selected baseline systems. The proposed SCPL algorithm consistently outperforms the baseline systems by approximately 5% to 25% in general. Most importantly, the HEES system using the proposed SCPL algorithm improves the energy harvesting ability by up to 48% compared to the BBF policy, which ignores the supercapacitor banks. This explains the poor performance of a homogeneous EES system of the same battery banks.

Tables IV and V show that the SBF policy generally performs well with a smaller number of PV modules, e.g., configuration of 4×2 or 2×4, or lower solar irradiance level, e.g., in December. In this case, the supercapacitor banks have enough capacity to accommodate all energy generated by the PV modules. Hence, the SBF policy takes the advantage of the high charging efficiency of the supercapacitor banks. However, SBF policy suffers from serious performance degradation later on after the supercapacitor banks are fully charged, as shown in the test cases for April and July with 4×6 or 6×6 PV modules. In contrast, UB policy achieves good results for those test cases with large amount of energy generation because it unbiasedly allocates generated energy to all EES banks. The performance of UB policy is quite close to the proposed SCPL algorithm in some corner cases because even the best energy allocation does not help much when the energy generation rate is too high. However, in general, the proposed SCPL algorithm outperforms UB policy by fully utilizing the high-efficiency EES banks.

Since the optimal V_{cti} depends on the energy generation profile, charge allocation policy, SoCs, and properties of EES banks, there is no way to determine a generally optimal V_{cti}. We observe a fluctuation of the total energy gain up to 20.7% in case of the different V_{cti} settings in Tables IV and V. Hence, it is not surprising that an inappropriate V_{cti} can be often used in practice unless the proposed concept is widely accepted. In contrast, the proposed SCPL algorithm searches and converges rapidly to the optimal V_{cti}.

Fig. 11(a) shows the total instantaneous power gain of all the EES banks in the eight-bank HEES system during the 12 h charge allocation process. The SBF policy performs well at the beginning but suffers from a huge performance degradation after all supercapacitor banks are fully charged. Fig. 11(b) and (c) shows that the average array charging currents of supercapacitor banks drop to zero and the currents of battery banks jump high at 1 PM. The SBF policy harvests less energy than BBF policy afterward due to higher self-discharge from the fully charged supercapacitor banks. The UB and BBF policies allocate charging power uniformly to all the EES banks as shown in Fig. 8. The proposed SCPL algorithm activates the supercapacitor banks at 7 AM according to the solar irradiance level and fully charges the supercapacitor banks at 4 PM. Fig. 11(a) shows that SCPL algorithm outperforms the other
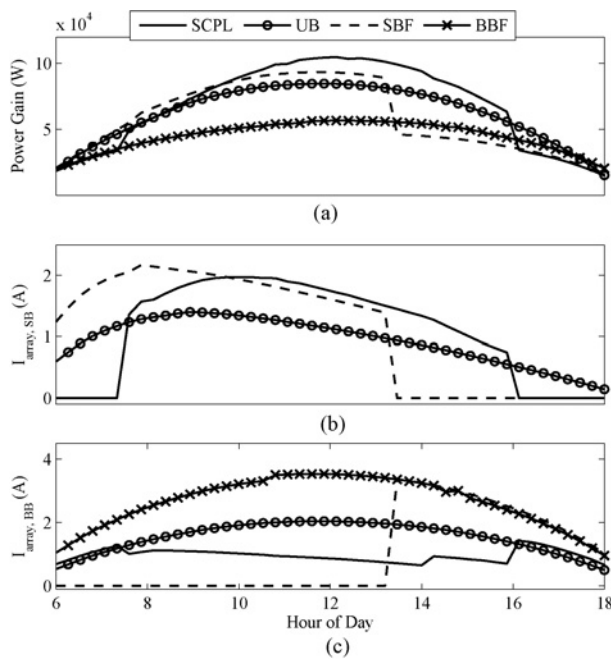
Fig. 11. Comparison of (a) total power gain, (b) average array charging current of supercapacitor banks, and (c) battery banks in the eight-bank HEES system with the 4×6 PV module. Simulated using solar data in Los Angeles in July.

baseline systems by properly allocating charging power and determining the CTI voltage.

VI. CONCLUSION

The HEES system is one of the most promising and practical ways to achieve a high-performance and low-cost EES system. This was the first paper that introduces fundamental concepts of GCA, including the system architecture and formal problem definition. The GCA problem was formulated as a mixed-integer nonlinear optimization problem. We proposed a systematic algorithm for the GCA problem by solving a series of constrained ICA at each decision epochs with time-dependent power limits to avoid the greedy decisions. Furthermore, we proposed an effective way to solve the ICA problem and achieve a near-optimal solution in an iterative manner. In each iteration, we solved a standard convex optimization problem in polynomial time. We performed simulations for HEES systems using PV modules as the power source and demonstrated that the proposed algorithm generally improves the energy harvesting ability by 5% to 25% against the baseline setups.

REFERENCES

[1] Q. Xie, Y. Wang, Y. Kim, N. Chang, and M. Pedram, "Charge allocation for hybrid electrical energy storage systems," in *Proc. Int. Conf. Hardware/Softw. Codesign Syst. Synthesis*, 2011, pp. 277–284.

[2] H. T. Odum, "Energy quality and carrying capacity of the earth," *Tropical Ecol.*, vol. 16, no. 1, pp. 1–8, 1975.

[3] J. Baker and A. Collinson, "Electrical energy storage at the turn of the millennium," *Power Eng. J.*, vol. 13, no. 3, pp. 107–112, Jun. 1999.

[4] T. Moore and J. Douglas, "Energy storage, big opportunities on a smaller scale," *EPRI J.*, pp. 16–23, Spring. 2006.

[5] D. H. Doughty, P. C. Butler, A. A. Akhil, N. H. Clark, and J. D. Boyes, "Batteries for large-scale stationary electrical energy storage," *Elecrochem. Soc. Interface*, vol. 19, no. 3, pp. 49–53, 2010.

[6] Y. Wang, S. Yue, L. Kerofsky, N. Chang, and M. Pedram, "A hierarchical control algorithm for managing electrical energy storage systems in homes equipped with PV power generation," in *Proc. IEEE Green Technol. Conf.*, Apr. 2012, pp. 1–6.

[7] I. Koutsopoulos, V. Hatzi, and L. Tassiulas, "Optimal energy storage control policies for the smart power grid," in *Proc. IEEE Int. Conf. Smart Grid Commun.*, Oct. 2011, pp. 475–480.

[8] M. Pedram, N. Chang, Y. Kim, and Y. Wang, "Hybrid electrical energy storage systems," in *Proc. 16th ACM/IEEE Int. Symp. Low Power Electron. Des.*, Aug. 2010, pp. 363–368.

[9] F. Koushanfar, "Hierarchical hybrid power supply networks," in *Proc. 47th ACM/IEEE Des. Autom. Conf.*, Jun. 2010, pp. 629–630.

[10] Y. Wang, Q. Xie, Y. Kim, N. Chang, and M. Pedram, "Charge migration effciency optimization in hybrid electrical energy storage (HEES) systems," in *Proc. Int. Symp. Low Power Electron. Des.*, Aug. 2011, pp. 103–108.

[11] Y. Kim, S. Park, Y. Wang, Q. Xie, N. Chang, M. Poncino, and M. Pedram, "Balanced reconfiguration of storage banks in a hybrid electrical energy storage system," in *Proc. IEEE/ACM Int. Conf. Comput.-Aided Des.*, Nov. 2011, pp. 624–631.

[12] Q. Xie, Y. Wang, Y. Kim, D. Shin, N. Chang, and M. Pedram, "Charge replacement in hybrid electrical energy storage systems," in *Proc. 17th Asia South Pacific Des. Autom. Conf.*, Jan.–Feb. 2012, pp. 627–632.

[13] Y. Wang, Q. Xie, M. Pedram, Y. Kim, N. Chang, and M. Poncino, "Multiple-source and multiple-destination charge migration in hybrid electrical energy storage systems," in *Proc. Des., Autom Test Eur. Conf. Exhib.*, Mar. 2012, pp. 169–174.

[14] Q. Xie, X. Lin, Y. Wang, M. Pedram, D. Shin, and N. Chang, "State of health aware charge management in hybrid electrical energy storage systems," in *Proc. Des., Autom Test Eur. Conf. Exhib.*, Mar. 2012, pp. 1060–1065.

[15] Y. Kim, S. Park, N. Chang, Q. Xie, Y. Wang, and M. Pedram, "Networked architecture for hybrid electrical energy storage systems," in *Proc. ACM/EDAC/IEEE Des. Autom Conf.*, Jun. 2012, pp. 522–528.

[16] Q. Xie, D. Zhu, Y. Wang, Y. Kim, N. Chang, and M. Pedram, "An efficient scheduling algorithm for multiple charge migration tasks in hybrid electrical energy storage systems," in *Asia South Pacific. Des. Autom. Conf.*, Jan. 2013, pp. 749–754.

[17] C. Holland, J. Weidner, R. A. Dougal, and R. E. White, "Experimental characterization of hybrid power systems under pulse current loads," *J. Power Sources*, vol. 109, no. 1, pp. 32–37, 2002.

[18] M. D. Zolot and B. Kramer, "Hybrid energy storage studies using batteries and ultracapacitors for advanced vehicles," Presented to the 12th International Seminar on Double Layer Capacitors and Similar Energy Storage Devices, Dec. 2002.

[19] L. Gao, R. Dougal, and S. Liu, "Power enhancement of an actively controlled battery/ultracapacitor hybrid," *IEEE Trans. Power Electron.*, vol. 20, no. 1, pp. 236–243, Jan. 2005.

[20] R. Schupbach and J. C. Balda, "The role of ultracapacitors in an energy storage unit for vehicle power management," in *Proc. Veh. Technol. Conf.*, Oct. 2003, pp. 3236–3240.

[21] L. Solero, A. Lidozzi, and J. A. Pomilio, "Design of multiple-input power converter for hybrid vehicles," *IEEE Trans. Power Electron.*, vol. 20, no. 5, pp. 1007–1016, Sep. 2005.

[22] R. A. Dougal, S. Liu, and R. E. White, "Power and life extension of battery–ultracapacitor hybrids," *IEEE Trans. Compon. Packag. Technol.*, vol. 25, no. 1, pp. 120–131, Mar. 2002.

[23] G. Sikha and B. N. Popov, "Performance optimization of a battery-ultrapacitor hybrid system," *J. Power Sources*, vol. 134, no. 1, pp. 130–138, 2004.

[24] Y. Kim, N. Chang, Y. Wang, and M. Pedram, "Maximum power transfer tracking for a photovoltaic-supercapacitor energy system," in *Proc. 16th ACM/IEEE Int. Symp. Low Power Electron. Des.*, Aug. 2010, pp. 307–312.

[25] Solar Resource and Meteorological Assessment Project (SOLRMAP) [Online]. Available: http://www.nrel.gov/midc/lmu/

[26] W. Lee, Y. Kim, Y. Wang, N. Chang, M. Pedram, and S. Han, "Versatile high-fidelity photovoltaic module emulation system," in *Proc. Int. Symp. Low Power Electron. Des.*, Aug. 2011, pp. 91–96.

[27] P. Rong and M. Pedram, "An analytical model for predicting the remaining battery capacity of lithium-ion batteries," *IEEE Trans. Very Large Scale Integr. Syst.*, vol. 14, no. 5, pp. 444–451, May 2006.

[28] D. Rakhmatov, "Battery voltage modeling for portable systems," *J. ACM Trans. Des. Autom. Electron. Syst.*, vol. 14, no. 2, pp. 1–36, 2009.

[29] L. Benini, G. Castelli, A. Macii, E. Macii, M. Poncino, and R. Scarsi, "Discrete-time battery models for system-level low-power design," *IEEE Trans. Very Large Scale Integr. Syst.*, vol. 9, no. 5, pp. 639–640, Oct. 2001.

[30] M. Chen and G. Rincon-Mora, "Accurate electrical battery model capable of predicting runtime and I–V performance," *IEEE Trans. Energy Convers.*, vol. 21, no. 2, pp. 504–511, Jun. 2006.

[31] D. Shin, Y. Wang, Y. Kim, J. Seo, M. Pedram, and N. Chang, "Battery-supercapacitor hybrid system for high-rate pulsed load applications," in *Proc. Des., Autom. Test Eur. Conf. Exhib.*, Mar. 2011, pp. 1–4.

[32] D. Linden and T. B. Reddy, *Handbook of Batteries*. New York: McGraw-Hill, 2001.

[33] H. Chen, T. N. Cong, W. Yang, C. Tan, Y. Li, and Y. Ding, "Progress in electrical energy storage system: A critical review," *Progr. Natural Sci.*, vol. 19, no. 3, pp. 291–312, Mar. 2009.

[34] Y. Choi, N. Chang, and T. Kim, "DC–DC converter-aware power management for low-power embedded systems," *IEEE Trans. Comput.Aided Des. Integr. Circuits Syst.*, vol. 26, no. 8, pp. 1367–1381, Aug. 2007.

[35] (Linear Technology Corporation). (2008). LTM4607—36Vin, 24Vout high efficiency buck-boost dc/dc μmodule [Online]. Available: http://www.linear.com/product/LTM4607

[36] R. E. Bird and R. L. Hulstrom, "Simplified clear sky model for direct and diffuse insolation on horizontal surfaces." U.S. Solar Energy Research Institute, Golden, CO, Tech. Rep. SERI/TR-642-761, 1981.

[37] J. Shim, R. Kostecki, T. Richardson, X. Song, and K. Striebel, "Electrochemical analysis for cycle performance and capacity fading of a lithium-ion battery cycled at elevated temperature," *J. Power Sources*, vol. 112, no. 1, pp. 222–230, 2002.

[38] L. Lam, P. Bauer, and E. Kelder, "A practical circuit-based model for li-ion battery cells in electric vehicle applications," in *Proc. IEEE 33rd Int. Telecommun. Energy Conf.*, Oct. 2011, pp. 1–9.

[39] B. Y. Liaw, E. P. Roth, R. G. Jungst, G. Nagasubramanian, H. L. Case, and D. H. Doughty, "Correlation of Arrhenius behaviors in power and capacity fades with cell impedance and heat generation in cylindrical lithium-ion cells," *J. Power Sources*, vols. 119–121, pp. 874–886, Jun. 2003.

[40] A. Millner, "Modeling lithium ion battery degradation in electric vehicles," in *Proc. IEEE Conf. Innov. Technol. Efficient Rel. Elect. Supply*, Sep. 2010, pp. 349–356.

[41] Gold Peak Industries, San Diego, CA, GP batteries datasheet: Model GP1051L35, 2011.

[42] Maxwell Technologies, San Diego, CA, BCAP0650 P270 K04, 2010.

Massoud Pedram (F'01) received the B.S. degree in electrical engineering from the California Institute of Technology, Pasadena, CA, USA in 1986, and the M.S. and Ph.D. degrees in electrical engineering and computer sciences from the University of California, Berkeley, CA, USA in 1989 and 1991, respectively.

He then joined the Department of Electrical Engineering Systems, University of Southern California, Los Angeles, CA, USA where he is currently a Professor and the Chair of computer engineering. He has published four books and more than 400 journal and conference papers. His current research interests include energy-efficient computing, energy storage systems, low power electronics and design, and computer-aided design of VLSI circuits and systems.

Dr. Pedram has served on the technical program committee of a number of conferences, including the Design Automation Conference, Design and Test in Europe Conference, and the International Conference on Computer Aided Design. He cofounded and served as the Technical Co-Chair and General Co-Chair of the International Symposium on Low Power Electronics and Design in 1996 and 1997, respectively. He was the Technical Program Chair and the General Chair of the International Symposium on Physical Design, in 2002 and 2003, respectively. He is a recipient of a number of Best Paper Awards, including two from the IEEE TRANSACTIONS ON COMPUTER-AIDED DESIGN OF INTEGRATED CIRCUITS AND SYSTEMS and the IEEE TRANSACTIONS ON VERY LARGE SCALE INTEGRATION SYSTEMS. He is the recipient of the National Science Foundation's Young Investigator Award in 1994 and the Presidential Faculty Fellow Award in 1996. He currently serves as the Editor in Chief of the ACM Transactions on Design Automation of Electronic Systems and the IEEE JOURNAL ON EMERGING AND SELECTED TOPICS IN CIRCUITS AND SYSTEMS.

Qing Xie (S'12) received the B.S. degree in physics from Fudan University, Shanghai, China, in 2007, and the M.S. degree from Northeastern University, Boston, MA, USA, in 2009. He is currently pursuing the Ph.D. degree from the Department of Electrical Engineering, University of Southern California, Los Angeles, under the supervision of Prof. M. Pedram.

His current research interests include the area of low-power systems design, energy storage systems, system-level power management, thermal management, and near-threshold computing.

Mr. Xie is a recipient of the Best Paper Award from the 30th IEEE International Conference on Computer Design.
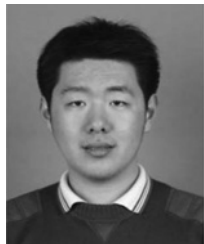
Yanzhi Wang (S'12) received the B.S. degree (with distinction) in electronic engineering from Tsinghua University, Beijing, China, in 2009. He is currently pursuing the Ph.D. degree in electrical engineering from the University of Southern California, Los Angeles, under the supervision of Prof. M. Pedram.

His current research interests include system-level power management, next-generation energy sources, hybrid electrical energy storage systems, near-threshold computing, and the smart grid. He has published 40 papers in these areas.

Younghyun Kim (M'13) received the B.S. degree (with the highest Hons.) in computer science and engineering and the Ph.D. degree in electrical engineering and computer science from Seoul National University, Seoul, Korea, in 2007 and 2013, respectively.

He was a Visiting Scholar with the University of Southern California, Los Angeles, CA, USA from 2009 to 2010, and in 2011. He is currently with the Department of Electrical Engineering and Computer Science, Seoul National University. His current research interests include embedded system design, system-level power management, next-generation energy sources, and hybrid electrical energy storage systems.

Dr. Kim was the Low Power Design Contest Winner at the International Symposium on Low Power Electronics and Design in 2007 and 2012, and received the IEEE Solid-State Circuits Society Seoul Chapter Best Paper Award at the International SoC Design Conference in 2009.

Naehyuck Chang (F'12) received the B.S., M.S., and Ph.D. degrees from the Department of Control and Instrumentation, Seoul National University, Seoul, Korea, in 1989, 1992, and 1996, respectively.

In 1997, he joined the Department of Computer Engineering, Seoul National University, where he is currently a Professor with the Department of Electrical Engineering and Computer Science, and the Vice Dean of the College of Engineering. His current research interests include low-power embedded systems, hybrid electrical energy storage systems, and next-generation energy sources.

Dr. Chang serves on the technical program committees in many electronic design automation conferences, including Design Automation Conference (DAC), the International Conference on Computer-Aided Design (ICCAD), the International Symposium on Low Power Electronics and Design (ISLPED), Design, Automation, and Test in Europe, the International Conference on Hardware-Software Codesign and System Synthesis (CODES+ISSS), and the Asia and South Pacific Design Automation Conference (ASP-DAC). He was a technical program committee (TPC) Co-Chair of the IEEE International Conference on Embedded and Real-Time Computing Systems and Applications 2007, ISLPED 2009, Embedded Systems for Real-Time Multimedia (ESTIMedia) 2009 and 2010, and CODES+ISSS 2012, and will serve as the TPC Chair of the International Conference on Computer Design 2014 and ASP-DAC 2015. He was the General Vice Chair of the ISLPED 2010, and the General Chair of the ISLPED 2011 and ESTIMedia 2011. He is an Associate Editor of the IEEE TRANSACTIONS ON CIRCUITS AND SYSTEMS——PART I: REGULAR PAPERS, the IEEE TRANSACTIONS ON COMPUTER-AIDED DESIGN OF INTEGRATED CIRCUITS AND SYSTEMS, Association for Computing Machinery (ACM) Transactions on Design Automation of Electronic Systems (TODAES), and ACM Transactions on Embedded Computing Systems (TECS), Springer Design Automation for Embedded Systems. He was the Guest Editor of ACM TODAES in 2010, and ACM TECS in 2010 and 2011. He is the ACM Special Interest Group on Design Automation Chair and an ACM Distinguished Scientist.